Hindawi Publishing Corporation
Journal of Nanomaterials
Volume 2015, Article ID 575401, 5 pages
http://dx.doi.org/10.1155/2015/575401

Research Article

Structural and Magnetic Properties of $Ni_{81}Fe_{19}$ Thin Film Grown on Si(001) Substrate via Single Graphene Layer

Gui-fang Li, Shibin Liu, Shanglin Yang, and Yongqian Du

School of Electronics and Information, Northwestern Polytechnical University, 127 West Youyi Road, Xi'an, Shaanxi 710072, China

Correspondence should be addressed to Gui-fang Li; gfli@nwpu.edu.cn

Received 10 December 2014; Accepted 5 February 2015

Academic Editor: Yuanlie Yu

We prepared magnetic thin films $Ni_{81}Fe_{19}$ on single-crystal Si(001) substrates via single graphene layer through magnetron sputtering for $Ni_{81}Fe_{19}$ and chemical vapor deposition for graphene. Structural investigation showed that crystal quality of $Ni_{81}Fe_{19}$ thin films was significantly improved with insertion of graphene layer compared with that directly grown on Si(001) substrate. Furthermore, saturation magnetization of $Ni_{81}Fe_{19}$/graphene/Si(001) heterostructure increased to 477 emu/cm^3 with annealing temperature $T_a = 400^\circ$C, which is much higher than values of $Ni_{81}Fe_{19}$/Si(001) heterostructures with T_a ranging from 200°C to 400°C.

1. Introduction

Efficient and robust injection of spin polarized electrons into semiconductor channel and manipulating the injected spin electrons have been persistent problems for semiconductor-based spintronic devices [1–3]. Hanle effect curves from ferromagnetic metal into semiconductor channel by three-terminal geometry have been reported [4–7]; moreover, the spin valve signals from ferromagnetic metal into semiconductor channel were investigated by four-terminal geometry [8–10]; various insulator layers such as MgO, Al_2O_3, and SiO_2 were inserted between ferromagnetic metal and semiconductor to solve the conductance mismatch problem [11–14]. Although clear Hanle signals were obtained for three-terminal geometry in ferromagnetism/insulator/semiconductor system, the high contact resistance area products resulting from the insulator layer were a serious issue [15].

Graphene was a potential candidate for an insulator tunneling barrier because (1) it exhibited poor conductivity perpendicular to the plane although it is very conductive in plane [16] and (2) it is a highly uniform, defect-free, and thermally stable layer. Cobas et al. reported that clear magnetoresistance curves were obtained for graphene-based magnetic tunneling junctions in which graphene works as a tunneling barrier [17]. van't Erve et al. reported spin injection from NiFe thin film into Si channel via graphene by three-terminal geometry [18]. However, the previous studies were restricted to the electrical properties of NiFe/graphene/Si heterostructures. The structural and magnetic properties of NiFe thin film grown on Si(001) substrate via graphene were rarely investigated.

Given this background, the purpose of the present study has been to fabricate $Ni_{81}Fe_{19}$/graphene heterostructures on Si(001) substrates and investigate their structural and magnetic properties. For this purpose, we prepared 50-nm thick $Ni_{81}Fe_{19}$ thin films on Si(001) substrate via single graphene layer by magnetron sputtering with various annealing temperature, T_a. We also prepared 50-nm thick $Ni_{81}Fe_{19}$ thin films directly grown on Si(001) substrates for comparison. The intensity of 111 peak and saturation magnetization significantly increased for $Ni_{81}Fe_{19}$ thin films compared with that directly grown on Si(001) substrate with $T_a = 400^\circ$C, indicating the improvement of crystal structure. These results demonstrated that the structural and magnetic properties of $Ni_{81}Fe_{19}$ thin film can be improved with insertion of graphene between ferromagnetic metal and semiconductor.

This paper is organized as follows. Section 2 describes materials and methods. Section 3 presents our experimental results regarding structural and magnetic properties of $Ni_{81}Fe_{19}$/graphene/Si(001) heterostructure and discussion. Section 4 summarizes our results and concludes.

2. Materials and Methods

Two kinds of layer structures were fabricated: firstly, (from the substrate side) graphene/$Ni_{81}Fe_{19}$ (50 nm)/AlO_x (1 nm) on a Si(001) single-crystal substrate. Grapehene was fabricated by chemical vapor deposition (CVD) on copper foil; then the copper foil was cut into the size of $20 \times 20\,mm^2$. Photoresist was coated on the surface of the graphene in order to assist the following wet-transfer process and add the copper foil into ferric trichloride to completely etch the copper. Then the photoresist-coated graphene was physically transferred on the Si(001) substrate which was cleaned by hydrofluoric acid solution and the photoresist was removed by acetone. Finally the sample was washed by deionized water. The prepared graphene/Si(001) substrate was installed in a high-vacuum chamber with base pressure of 5.0×10^{-4} Pa; the 50-nm thick $Ni_{81}Fe_{19}$ thin films were deposited by magnetron sputtering at room temperature (RT) and then subsequently annealing *in situ* at temperature $T_a = 400^\circ C$. Secondly, we also fabricated 50-nm thick $Ni_{81}Fe_{19}$ films directly grown on Si(001) at RT, which were annealed with T_a ranging from 200°C to 400°C.

We investigated the structural properties of the graphene through ALMEGA Dispersive Raman spectrometer (ALMEGA-TM) with a wavelength of 532 nm. The surface morphologies were observed using atomic force microscopy. The structural properties of $Ni_{81}Fe_{19}$ thin films were investigated by X-ray diffraction (XRD) θ-2θ scan. The magnetic properties of $Ni_{81}Fe_{19}$ thin films were investigated through vibrating sample magnetometer (VersaLab, Quantum Design) at RT.

3. Results and Discussion

3.1. Structural Properties of $Ni_{81}Fe_{19}$/Graphene/Si(001) Heterostructures. Firstly, we describe the structural properties of $Ni_{81}Fe_{19}$/graphene/Si(001) heterostructure. Figure 1 shows the Raman spectra of graphene on single-crystal Si(001) substrate. The typical G and 2D peak were observed at shift of 1596 cm^{-1} and 2685 cm^{-1}, respectively. The peak intensity ratio of I_{2D}/I_G is about 1.6; the higher peak intensity ratio for 2D peak compared with that of G peak indicated the graphene was single layer. Furthermore, the full width at half maximum (FWHM) of 2D peak was about 21 cm^{-1}, which is very close to the 25 cm^{-1} for the perfect single graphene layer. Although D peak was observed at shift of 1352 cm^{-1} which is related to the defect in the graphene layer, the peak intensity ratio $I_D/I_G \approx 0.06$ which is appreciably low, indicating the prepared graphene was almost defect-free [19].

Figure 2 shows the surface morphologies of $Ni_{81}Fe_{19}$ thin film on Si(001) substrate via single graphene layer by atomic force microscopy (AFM) measurements, the 50-nm thick $Ni_{81}Fe_{19}$ thin film had sufficiently flat surface morphologies with root mean square (rms) roughness of 0.47 nm, the $Ni_{81}Fe_{19}$ film was deposited at RT and subsequently annealed at 400°C on Si(001) substrate via graphene layer. This rms value was almost similar to that $Ni_{81}Fe_{19}$ thin film directly grown on MgO-buffered MgO substrate with value of 0.31 nm at annealing temperature T_a of 400°C.

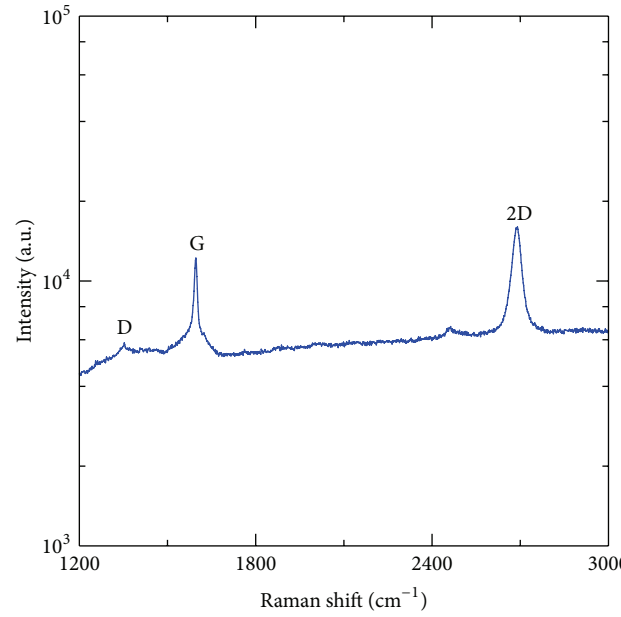

Figure 1: The Raman spectra of graphene on single-crystal Si(001) substrate.

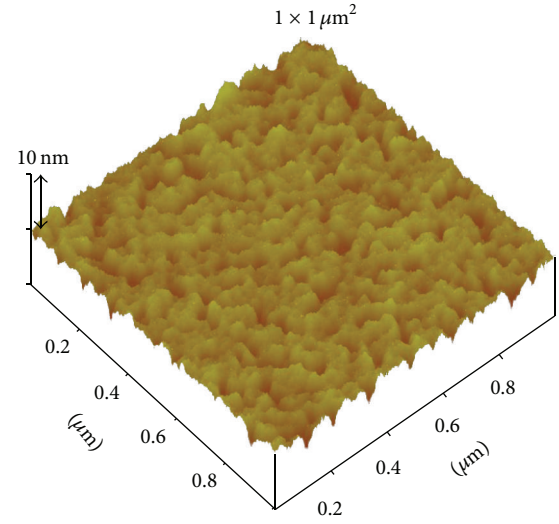

Figure 2: Three-dimensional AFM image ($1 \times 1\,\mu m^2$) of the surface topography of 50-nm thick $Ni_{81}Fe_{19}$ thin film on Si(001) substrate via single graphene annealed at 400°C.

Figure 3 shows X-ray diffraction patterns of 50-nm thick $Ni_{81}Fe_{19}$ films grown on Si(001) substrate via single graphene layer with annealing temperature of 400°C. The X-ray diffraction patterns of 50-nm thick $Ni_{81}Fe_{19}$ films directly grown on Si(001) were also shown for comparison, in which the $Ni_{81}Fe_{19}$ films were as-deposited and postdeposition annealed at temperature ranging from 200°C to 300°C. No appreciable peak was observed for the as-deposited $Ni_{81}Fe_{19}$ films, indicating that it was amorphous film. With increasing

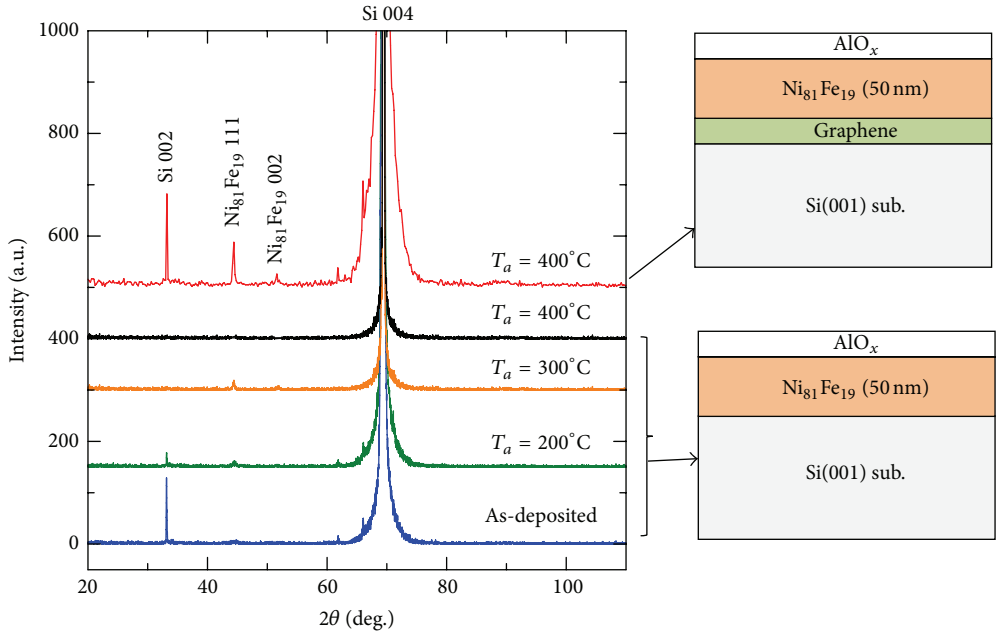

FIGURE 3: X-ray diffraction patterns of 50-nm thick $Ni_{81}Fe_{19}$ films grown on Si(001) substrate with various annealing temperature T_a, in which one set of curves indicate the $Ni_{81}Fe_{19}$/Si(001) heterostrcutres with T_a ranging from 200°C to 300°C and as-deposited $Ni_{81}Fe_{19}$ films, the other set of curve indicate the $Ni_{81}Fe_{19}$/graphene/Si(001) heterostrcutre with T_a = 400°C.

the annealing temperature, the 111 peak of $Ni_{81}Fe_{19}$ films appeared for T_a up to 200°C. In this sense, the crystal structure of the as-deposited $Ni_{81}Fe_{19}$ films was improved by the annealing. With continuous increasing the T_a to 300°C, 002 peak of $Ni_{81}Fe_{19}$ films was obtained and the intensity of 111 peak slightly increased compared with that for T_a = 200°C; however, the 002 peak of single-crystalline silicon substrate disappeared with T_a = 300°C, which was possibly due to the interdiffusion between $Ni_{81}Fe_{19}$ films and Si at relatively high annealing temperature. In order to confirm the supposition, the annealing temperature was increased up to 400°C. No appreciable 111 and 002 peaks of $Ni_{81}Fe_{19}$ films and 002 peak of silicon substrate were observed. The graphene was inserted between $Ni_{81}Fe_{19}$ films and Si(001) substrate as shown in Figure 3; the intensity of 111 and 002 peaks was significantly increased with T_a = 400°C and the interdiffusion between $Ni_{81}Fe_{19}$ films and Si(001) substrate was prevented; the crystal structure of $Ni_{81}Fe_{19}$ films was significantly improved by inserting graphene layer. Furthermore, the XRD patterns show that the heterostructure is composed of face centered cubic (fcc) structure, which is consistent with the fact that fcc structure is dominant in high Ni content $Ni_{81}Fe_{19}$ film [20].

3.2. Magnetic Properties of 50-nm Thick $Ni_{81}Fe_{19}$ Thin Films Grown on Si(001) Substrate via Single Graphene Layer. Next, we describe the magnetic properties of $Ni_{81}Fe_{19}$ thin films grown on Si(001) via graphene layer and that directly grown on Si(001) substrate. Figure 4(a) shows the magnetic hysteresis (M-H) curves of $Ni_{81}Fe_{19}$ thin films at 300 K. The M-H curve with T_a = 400°C was that $Ni_{81}Fe_{19}$ thin film grew on Si(001) substrate via graphene layer; the other two curves were those $Ni_{81}Fe_{19}$ thin films directly grown on Si(001) substrates. The magnetic field (H) was applied in the plane of the film along [100] direction of silicon substrate. The saturation magnetization (M_s) was 310 emu/cm^3 for $Ni_{81}Fe_{19}$ thin films deposited at RT without annealing; the M_s slightly increased to 350 emu/cm^3 with T_a = 300°C. The obtained M_s values were close to those $Ni_{81}Fe_{19}$ thin films grown on Ta and Ti substrate [21]. With increasing T_a up to 400°C, no appreciable M-H curve was observed for $Ni_{81}Fe_{19}$/Si(001) heterostructure, which was due to the nonnegligible interdiffusion between $Ni_{81}Fe_{19}$ thin film and Si(001) substrate. However, with insertion of the graphene between $Ni_{81}Fe_{19}$ films and Si(001) substrate, the M_s significantly increased up to 477 emu/cm^3 for T_a = 400°C, indicating that the magnetic properties of $Ni_{81}Fe_{19}$ thin film significantly improved.

Figure 4(b) shows the coercive force (H_c) for $Ni_{81}Fe_{19}$ thin film as a function of T_a. The H_c values at 300 K decreased with increasing T_a from H_c = 10 Oe for the as-deposited film to H_c = 3 Oe for T_a = 400°C. The decrease in H_c with increasing T_a was probably induced by a decrease in the pinning center density for the magnetic domain motion with increasing T_a up to 400°C [22].

4. Conclusion

We prepared $Ni_{81}Fe_{19}$ thin films grown on Si(001) substrate via graphene layer. First, the Raman spectra showed that the graphene was single layer and almost defect-free. Second, the X-ray pattern of $Ni_{81}Fe_{19}$/graphene/Si(001) heterostructure confirmed that the crystal quality of $Ni_{81}Fe_{19}$ thin films significantly increased with insertion of graphene single layer. Third, sufficiently flat surface morphologies were obtained for $Ni_{81}Fe_{19}$ thin films grown on Si(001) via graphene layer.

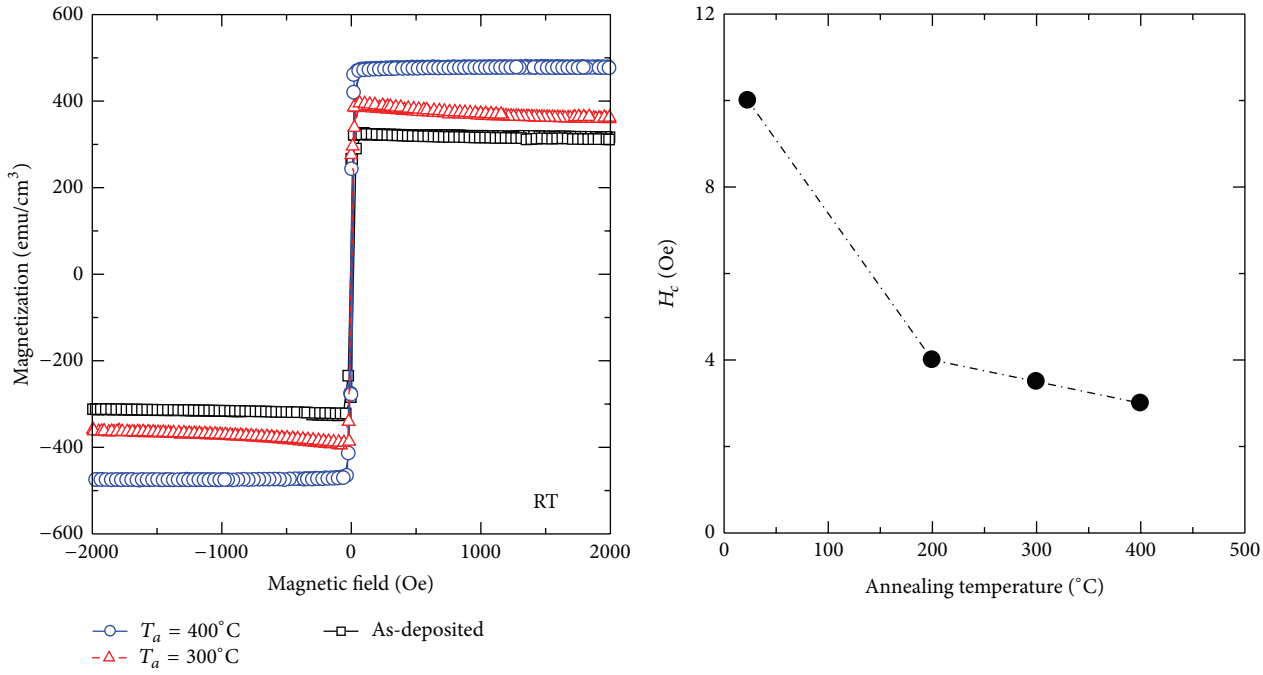

FIGURE 4: (a) Typical magnetic hysteresis curves for $Ni_{81}Fe_{19}$/graphene/Si(001) and $Ni_{81}Fe_{19}$/Si(001) heterostructures at 300 K with various T_a, where H was applied in the plane of the film along the $[100]_{Si}$ direction. (b) The coercive force (H_c) for $Ni_{81}Fe_{19}$ thin film as a function of T_a.

Fourth, relatively higher saturation magnetization values at 300 K were obtained for $Ni_{81}Fe_{19}$ thin films grown on Si(001) via graphene layer. These results confirmed that $Ni_{81}Fe_{19}$/graphene heterostructure is a potential candidate for spin injection source for spin injection into semiconductor channel.

Conflict of Interests

The authors declare that there is no conflict of interests regarding the publication of this paper.

Acknowledgment

This work was partly supported by The Fundamental Research Funds for the Central Universities (Grant no. 3102014JCQ01059), China.

References

[1] X. Lou, C. Adelmann, S. A. Crooker et al., "Electrical detection of spin transport in lateral ferromagnet-semiconductor devices," *Nature Physics*, vol. 3, no. 3, pp. 197–202, 2007.

[2] S. P. Dash, S. Sharma, R. S. Patel, M. P. De Jong, and R. Jansen, "Electrical creation of spin polarization in silicon at room temperature," *Nature*, vol. 462, no. 7272, pp. 491–494, 2009.

[3] M. Tran, H. Jaffrès, C. Deranlot et al., "Role of δ-hole-doped interfaces at ohmic contacts to organic semiconductors," *Physical Review Letter*, vol. 102, no. 3, Article ID 036601, 2009.

[4] K.-R. Jeon, B.-C. Min, I.-J. Shin et al., "Electrical spin accumulation with improved bias voltage dependence in a crystalline CoFe/MgO/Si system," *Applied Physics Letters*, vol. 98, no. 26, Article ID 262102, 2011.

[5] H. Saito, S. Watanabe, Y. Mineno et al., "Electrical creation of spin accumulation in *p*-type germanium," *Solid State Communications*, vol. 151, no. 17, pp. 1159–1161, 2011.

[6] A. Jain, L. Louahadj, J. Peiro et al., "Electrical spin injection and detection at Al_2O_3/*n*-type germanium interface using three terminal geometry," *Applied Physics Letters*, vol. 99, no. 16, Article ID 162102, 2011.

[7] I. A. Fischer, L.-T. Chang, C. Sürgers et al., "Hanle-effect measurements of spin injection from $Mn_5Ge_3C_{0.8}$/Al_2O_3-contacts into degenerately doped Ge channels on Si," *Applied Physics Letters*, vol. 105, no. 22, Article ID 222408, 2014.

[8] O. M. J. van't Erve, A. T. Hanbicki, M. Holub et al., "Electrical injection and detection of spin-polarized carriers in silicon in a lateral transport geometry," *Applied Physics Letters*, vol. 91, no. 21, Article ID 212109, 2007.

[9] T. Sasaki, T. Oikawa, T. Suzuki, M. Shiraishi, Y. Suzuki, and K. Noguchi, "Temperature dependence of spin diffusion length in silicon by Hanle-type spin precession," *Applied Physics Letters*, vol. 96, no. 12, Article ID 122101, 2010.

[10] Y. Zhou, W. Han, L.-T. Chang et al., "Electrical spin injection and transport in germanium," *Physical Review B*, vol. 84, no. 12, Article ID 125323, 2011.

[11] G. Schmidt, D. Ferrand, L. W. Molenkamp, A. T. Filip, and B. J. van Wees, "Fundamental obstacle for electrical spin injection from a ferromagnetic metal into a diffusive semiconductor," *Physical Review B: Condensed Matter and Materials Physics*, vol. 62, no. 8, pp. R4790–R4793, 2000.

[12] E. I. Rashba, "Theory of electrical spin injection: tunnel contacts as a solution of the conductivity mismatch problem," *Physical Review B: Condensed Matter and Materials Physics*, vol. 62, no. 24, Article ID R16267, pp. R16267–R16270, 2000.

[13] G.-F. Li, T. Taira, K.-I. Matsuda, M. Arita, T. Uemura, and M. Yamamoto, "Epitaxial growth of Heusler alloy Co_2MnSi/MgO heterostructures on Ge(001) substrates," *Applied Physics Letters*, vol. 98, no. 26, Article ID 262505, 2011.

[14] G.-F. Li, T. Taira, H.-X. Liu, K.-Z. Matsuda, T. Uemura, and M. Yamamoto, "Fabrication of fully epitaxial CoFe/MgO/CoFe magnetic tunnel junctions on Ge(001) substrates via a MgO interlayer," *Japanese Journal of Applied Physics*, vol. 51, no. 9, Article ID 093003, 2012.

[15] T. Uemura, K. Kondo, J. Fujisawa, K.-I. Matsuda, and M. Yamamoto, "Critical effect of spin-dependent transport in a tunnel barrier on enhanced Hanle-type signals observed in three-terminal geometry," *Applied Physics Letters*, vol. 101, no. 13, Article ID 132411, 2012.

[16] K. S. Krishnan and N. Ganguli, "Large anisotropy of the electrical conductivity of graphite," *Nature*, vol. 144, no. 3650, p. 667, 1939.

[17] E. Cobas, A. L. Friedman, O. M. J. van't Erve, J. T. Robinson, and B. T. Jonker, "Graphene as a tunnel barrier: graphene-based magnetic tunnel junctions," *Nano Letters*, vol. 12, no. 6, pp. 3000–3004, 2012.

[18] O. M. J. van't Erve, A. L. Friedman, E. Cobas, C. H. Li, J. T. Robinson, and B. T. Jonker, "Low-resistance spin injection into silicon using graphene tunnel barriers," *Nature Nanotechnology*, vol. 7, no. 11, pp. 737–742, 2012.

[19] G. Wang, M. Zhang, Y. Zhu et al., "Direct growth of graphene film on germanium substrate," *Scientific Reports*, vol. 3, article 2465, 2013.

[20] B. Liu, R. Huang, J. Wang et al., "Mössbauer investigation of Fe–Ni fine particles," *Journal of Applied Physics*, vol. 85, no. 2, pp. 1010–1013, 1999.

[21] S. Yang, S. Liu, B. Guo, W. Feng, and X. Hou, "Comparison of soft magnetic properties of $Ni_{81}Fe_{19}$ film with different substrates used for microfluxgate," *Micro & Nano Letters*, vol. 8, no. 10, pp. 602–605, 2013.

[22] E. C. Stoner and E. P. Wohlfarth, "A mechanism of magnetic hysteresis in heterogenous alloys," *Philosophical Transactions of the Royal Society A*, vol. 240, p. 599, 1948.